Mechatronics 53 (2018) 124–139

Contents lists available at ScienceDirect

Mechatronics

journal homepage: www.elsevier.com/locate/mechatronics

Control of TCP muscles using Takagi–Sugeno–Kang fuzzy inference system☆

Mohsen Jafarzadeh[a,b], Nicholas Gans[a], Yonas Tadesse[a,b,*]

[a] Department of Electrical and Computer Engineering, The University of Texas at Dallas, Richardson, TX 75080, USA
[b] Humanoid, Biorobotics and Smart Systems (HBS) Laboratory, Department of Mechanical Engineering, The University of Texas at Dallas, Richardson, TX 75080, USA

ARTICLE INFO

Keywords:
Actuators
Artificial muscles
Discrete-time state space
Fuzzy inference system
Digital control

ABSTRACT

Inspired by nature, many types of artificial muscles or actuators have been developed for mechatronic systems. Twisted and coiled polymer (TCP) muscles are some examples that are made from nylon or polyethylene. The muscles contract over 20% strokes under considerable load. There are limited studies available on the modeling and control of these muscles for practical use. In this paper, we show discrete-time modeling and control of the force of the muscles. Prediction error method (PEM) was used for parameter estimation of discrete-time state space models to find the order of the model. Then, proportional–integral (PI) controller was demonstrated as a classical controller to regulate the force of the muscles. To increase the speed of actuation, a Takagi–Sugeno–Kang (TSK) controller was employed as a fuzzy controller. Our experimental results demonstrate how the muscle can be controlled in practical settings and shows the superiority of TSK over the PI controller. We anticipate that the model and controllers will add new knowledge for the use of the twisted and coiled polymer muscle in mechatronic system.

1. Introduction

Actuators are essential elements in mechatronics systems and many types of actuators that mimic natural muscles have been proposed. Natural muscles are wonderful actuators, enabling humans to walk, quadrupeds to run, birds to fly, and fish to swim. Natural muscles are part of an integrated system that includes muscles, joints, sensors, ion delivery system, and a complex control system using neurons [1]. Studies on the contraction of natural muscles show their effectiveness [2]. Natural muscles have large strains; for example, a typical human muscle can contract more the 40% of its initial length [3]. Also, muscles demonstrate power density range from ~5 to 150 W/kg [4]. A natural muscle's conversion efficiency from adenosine triphosphate to mechanical energy is about 40%, which is what a typical car engine achieves [5].

Inspired by nature, many researchers have investigated several types of artificial muscles (also known as actuators). Shape memory alloys (SMA) [6–11], shape memory polymer (SMP) [12], dielectric elastomer [13], and pneumatic muscle [14–17] are examples of popular artificial muscles. In 2014, Haines et al. developed new artificial muscles that use fishing line and silver coated nylon as precursor materials [18]. To enable the polymer fibers to work as linear muscles, they twist and coil the polymer fibers by using a dead mass (m). These muscles can untwist when the stopper is removed (as shown in Fig 1). This problem can be solved by thermal annealing to set the structure and by forming torque-balanced structures. Fig. 1 shows a typical 1-ply TCP muscle fabrication steps using multifilament silver-coated nylon following the process of twisting, coiling, and annealing [19]. Different types of twisted and coiled polymer (TCP) muscles exhibit distinctive characteristics, they contract over 20% tensile stroke against a 35 MPa applied stress, and more importantly, these muscles provide hysteresis-free actuation compared to SMA actuators [18, 19]. Regarding cyclic tests, a 2-ply silver coated nylon 6,6 multifilament showed consistent strain for 5200 cycles when tested at 300 g load, 0.184 W/cm power input, and 0.03 Hz frequency [19]. TCP muscles have been used in many mechatronics systems such as a humanoid robot [20], prosthetic hands [21], a musculoskeletal system [22], energy harvester [23], rehabilitation [24], and forceps [25].

Accurate modeling and robust control of TCP muscles are essential for better understanding of these muscles and their practical use. Sharafi and Li introduced a phenomenological model that uses a Gaussian distribution function to formulate the actuation strain of the muscles [26]. However, they did not model the transient state of the TCP muscles. While hysteresis modeling of TCP muscles has been studied in [27–29], the hysteresis of these muscles is not significant as in isotonic testing (under constant load) [18, 19]. Therefore, a nonlinear controller is not required. The relationship between electrical impedance, deflection, force, and temperature of joule heated twisted and

☆ This paper was recommended for publication by Associate Editor Prof. T.H. Lee.

* Corresponding author.
E-mail address: Yonas.Tadesse@utdallas.edu (Y. Tadesse).

https://doi.org/10.1016/j.mechatronics.2018.06.007
Received 19 March 2018; Received in revised form 2 June 2018; Accepted 12 June 2018
Available online 22 June 2018
0957-4158/

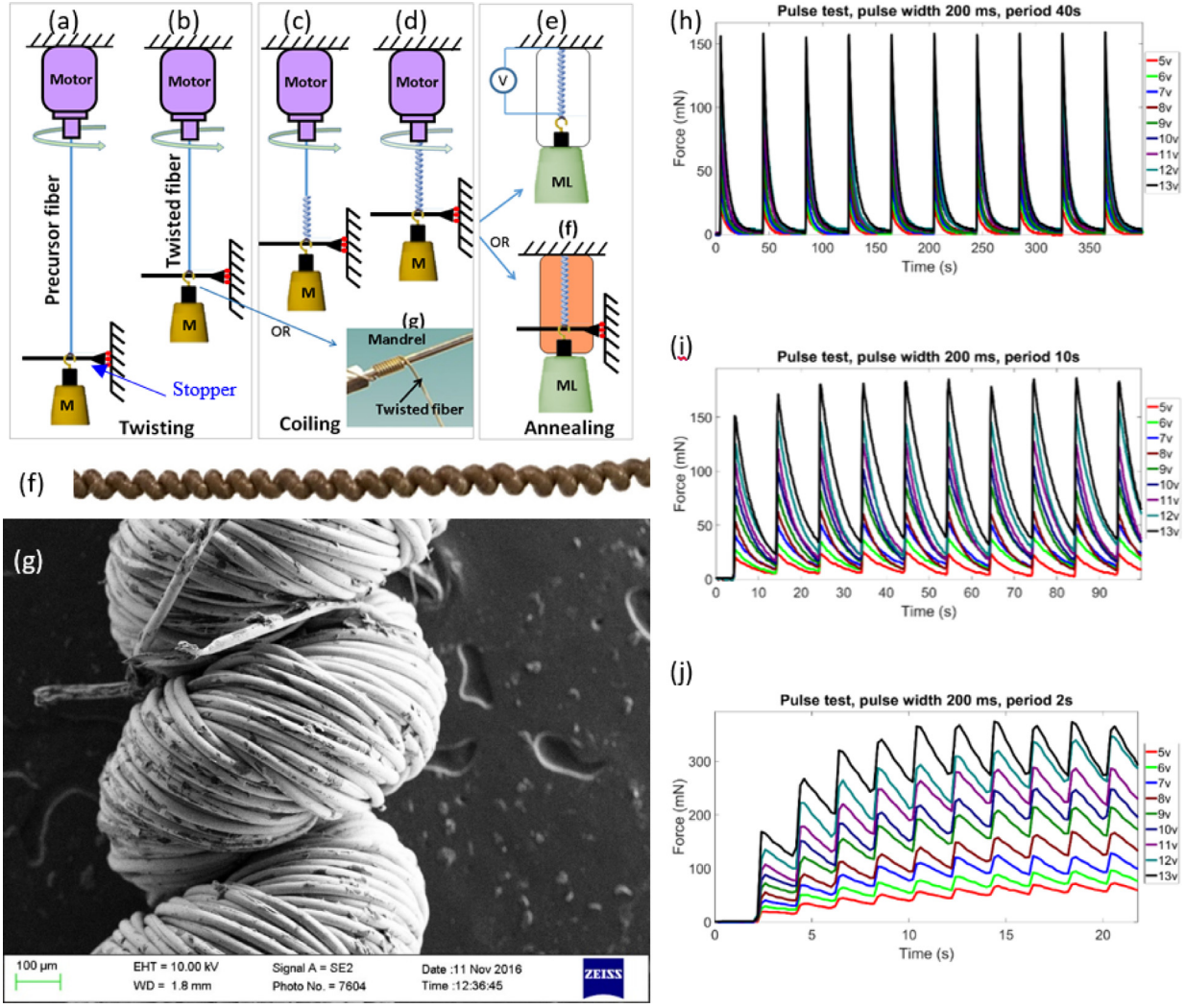

Fig. 1. Schematic diagram of the fabrication process for a 1-ply TCP muscle. (a) precursor fiber, (b) twisted fiber, (c) coiled fiber (d) fully coiled, and (e) annealing (f) the fabricated muscle (g) SEM image at high magnification. (h)–(i) cyclic actuation of 1-ply TCP muscle with pulse width 0.2 s ON and different periods.

coiled muscle (TCPM) has been examined in [30]. The muscle was made of fishing line wrapped with resistance wire and mandrel coiled to create spring-like structure. In [31, 32], a second order ODE was used to model displacement of the muscle. Edmonds and Trejos studied relations between the stiffness and temperature of a 2-ply silver coated twisted and coiled polymer (TCP_{Ag}) muscle [33]. The subscript Ag refers to the silver coating on the polymer. A physics based thermo-mechanical model of 1-ply TCP_{Ag} muscle has been investigated in [34]. The relationship between displacement and electrical resistance of the 1-ply TCP_{Ag} muscle is shown in [35]. In another study of TCP muscle, a finite element method is used for finding a mathematical model that describes the actuation in response to the temperature [36]. Karami and Tadesse proposed a multiphysics model for determining the displacement of TCP muscles as a function of the load and temperature. It is an algebraic model, except the temperature-electrical input relationship, which is put forward as a differential equation [37]. Even though these models provide insight into the muscle characteristics, they cannot be used for force control because they do not model and verify the dynamic relationship between the input electrical voltage and/or current and the output force.

In a related study, a feedforward (FF) controller based on the nonlinear model with the Hammerstein structure has been used for controlling the displacement of TCP actuator [38]. Their method is essentially an open-loop controller for the voltage and displacement. However, such a controller cannot compensate any disturbance. In another study, PID controller was used for displacement control of an antagonistic-type of TCP actuator [39]. An anti-windup compensator for TCP actuator can improve the behavior of the closed-loop system when the input (amplifier) is saturated [40]. Yip and Niemeyer reported that the relation between force and strain of a twisted and coiled polymer muscle represents a classic hysteretic behavior. For control of the muscle, they modeled the muscle as a linear system like a spring and damper combined with the thermal constant. They used a first order linear time invariant (LTI) system to model the thermo-electrical behavior of the muscle. A gray box system identification method was used to find the parameters of the model. Then, they used a lead and feedforward-proportional controllers to regulate the force of muscle [41, 42]. Although their controller tracked the desired force, they did not analyze the sensitivity of the controllers to disturbance and errors in model parameters.

There are four important research gaps in modeling and control of TCP actuators: (1) determining the force of an actuator in response to voltage for different geometries, (2) modeling the system in observable form and discrete-time, (3) designing digital controllers, and (4) increasing the speed of actuation without decreasing the actuator lifetime. The objective of this study is to control the force of a TCP actuator in a short period (i.e., small settling time), without applying high voltage and without breaking the actuator. In addition, the controllers

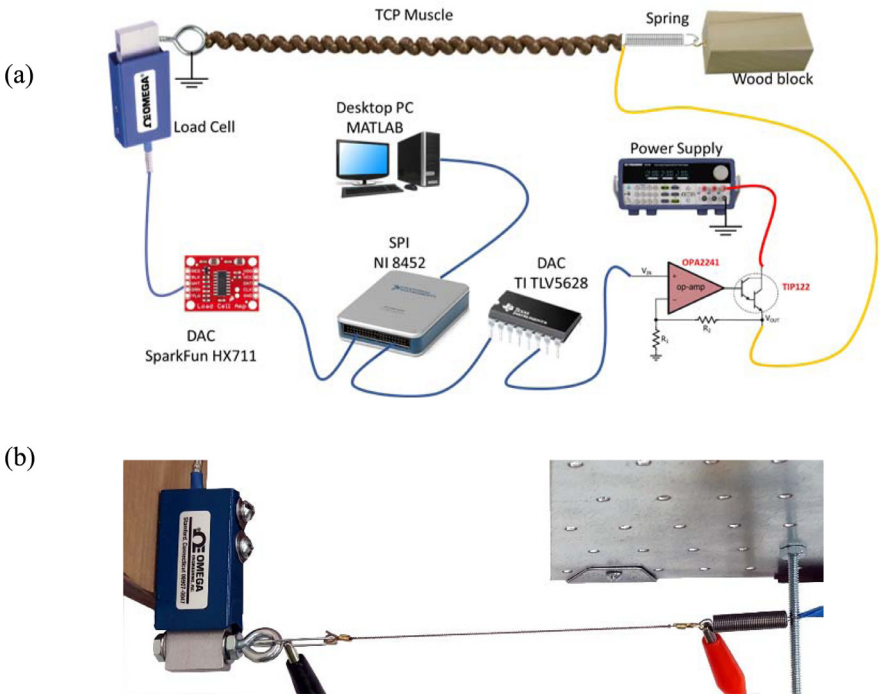

Fig. 2. Experimental setup for modeling and control of 1-ply TCP (a) schematic and (b) photograph of the actual setup focusing on the TCP actuator and end connection.

must run in a commonly available digital microprocessor/microcontroller using analog to digital converter (ADC) and digital to analog converter (DAC) for practical implementation. Moreover, the controllers must be robust and work in the presence of sensor noise and disturbance. Our methodology is to use black-box system identification to find the order of the actuator, model the system as a discrete-time state space system, estimate the state space parameters with the prediction error method (PEM), use a digital PI controller to ensure a robust closed-loop system and short time to steady-state, and use Takagi–Sugeno–Kang (TSK) to design a faster digital controller.

The main contribution of this paper is combining the proportional–integral (PI) controller with linguistic rules to obtain a fuzzy controller to regulate the force of TCP muscles/actuators. We used the fuzzy controller to speed up the system response without increasing maximum applied voltage to the TCP actuator and without adding a significant amount of overshoot. For designing the fuzzy controller, the TSK view of a fuzzy inference system was used and verified theoretically as well as experimentally. A load cell was used to sense the force of the actuator. The data from the load cell was read by an ADC, which was connected to a computer via a Serial Peripheral Interface (SPI) bus. In each time step, the error was calculated by subtracting the measured force from the desired force. Then, Gaussian membership functions was used for fuzzification of error (measured force – desired force). Essentially, the fuzzy inference system consists of three rules. The first rule enforces zero voltage when the measured force is much more than desired force (large negative error). The second rule applies PI controller when the error is small. The third rule gives the maximum voltage to the actuator when the measured force is very small than the desired force (large positive error) to increase the response speed of the closed-loop system. In our case, weighted average defuzzification was used to compute the applied voltage. A digital to analog converter was used for generating the scaled-down magnitude of the computed voltage. Then, the generated voltage was amplified with a single-supply rail-to-rail precision Op-Amp and power Darlington Bipolar Junction Transistor (BJT) to produce the applied voltage (to the actuator). The fuzzy controller demonstrates superiority over the classical controller in both simulation and experiments for controlling the force of TCP actuators. The proposed controller regulates the force of the muscle in the presence of sensor noise (vibration and reading noise) and disturbance (e.g., air flow).

This paper is organized as follows. First, the modeling and system identification of the TCP muscles are explained in Section 2. Then, control force of the muscle in closed-loop by using classical controllers and fuzzy controller, Takagi–Sugeno–Kang view of a fuzzy inference system, are stated in Section 3. In Section 4, results of classical controllers and the fuzzy controller are demonstrated. Section 5 illustrates an application of these controllers. The last section is a conclusion for modeling and controlling of the force of the TCP muscles.

2. TCP muscles/actuators preparation and testing

To model and control the new TCP actuators, first the muscles were fabricated and experiments were performed to determine the system parameters. In this paper, commercially available sewing thread (Shieldex PN#260151023534oz) was used as a precursor material for fabricating TCP muscles. The precursor material has 136 filaments, nominal diameter of 0.2 mm, electrical resistance of 0.50 Ω/cm, and linear density of 1.3 mg/cm. It consists of a multifilament silver-coated nylon 6,6 sewing thread as shown earlier in the scanning electron microscope (SEM) image in Fig. 1. The silver-plated layer enables the nylon 6,6 sewing thread to be actuated by electrical power. The electrical power causes Joule heating of the muscle and hence enabling contraction. The TCP muscles are produced by twisting, coiling, annealing, and training. As Fig. 1 illustrates, 4 steps are required to create a TCP muscle. The first step is twist insertion (Fig. 1a–b). In this step, the muscle is attached to a motor while the other end is tethered to a weight. At the bottom, a stopper is also necessary to prevent the precursor fiber from untwisting [18, 19]. In the next step, coiling is induced by over insertion of twist into the fiber as shown in (Fig. 2c and d) either self-coiling or coiling over a mandrel. To obtain a good and consistent performance, appropriate annealing and training (Fig. 1e) are required. The aim of the annealing is to lock the shape of the muscle, otherwise the muscle will untwist. The stopper cannot be removed until the annealing step is finished. In this study, the muscles are

annealed electro-thermally by applying electrical power to the muscles (Fig. 1e above), which result in heating. The amplitude of power determines the magnitude of temperature rise in the muscles and hence the stroke of the muscle. The last step is to perform the training to obtain repeating actuation cycles.

Fig. 1(h)–(i) shows the cyclic pulse response of a 1-ply muscle. In this experiment, on-time was 0.2 s and periods were 2, 10, and 40 s. In the low-frequency pulse actuation, the muscle has enough time to cool down. By increasing the frequency, the pulse response behaves like a step response. This is because heat is accumulated in the muscle, and such response is a typical behavior of thermal actuators. This is also the reason thermal muscles are slow actuators. Therefore, the desired trajectory should be slow enough such that the muscle can follow it.

3. Modeling and system identification

In the literature, the common assumption in the modeling of TCP muscle is that the muscle acts like a mechanical spring that has variable stiffness depending on the supplied electrical power. Therefore, the relation between voltage square value, as system input, and the force of the muscle, as system output, was modeled by a first order differential equation (1st ODE) [41, 42]. Although this model shows very high fitness, other models should be investigated by comparing this model with other models, such as black box system identification to find the order and parameters of the system [43].

The TCP muscles require a pretension force to actuate considerably. In this work, a passive spring with a stiffness of 52.5 N/m was used to provide the pretension. The TCP muscles, 1-ply, had a diameter of 0.8 mm and a length of 110 mm; a pre-stress of 1 N was applied by stretching the spring. Fig. 2 demonstrates the experimental setup which includes a load cell, a power supply (Topward 6306D), a National Instrument's serial peripheral interface (NI USB-8452 SPI), a load cell amplifier, an analog to digital converter (SparkFun HX711), and a digital to analog converter (Texas Instrument TLV5628). The load cell was Omega LCEB-5 with 3 mv/v rated output, 7 mN linearity, 5 mN hysteresis, and 3 mN repeatability. Also, an op-amp (TI OPA2241) and a BJT (ST TIP 122) were used as amplifiers for the circuit to increase current and voltage between the digital to analog converter (DAC) and the muscle. All controllers were implemented on a desktop with MATLAB R2017a 64 bit (Table 1).

Experiments on 1-ply TCP have shown that the steady-state relationship between electrical power and the force of the muscle is closed to linear; however, there exist small amount of error about 5% error. Also, the steady-state relation between voltage square (V^2) and the force of the muscle is close to linear with 10% error. The main reason for such difference in accuracy is that the resistance of the muscle changes during the actuation, due to the change in the temperature of the muscle. This means, by assuming a constant electrical resistance of the muscle during actuation, the accuracy of the model decreases from 95% to 90% [43]. However, in practice, controlling the voltage is easier and cheaper than controlling the electrical power of the muscles. Also, 90% fitness of a model is sufficient to use the model to design a controller. Therefore, in this paper, the voltage square value was used as the input of the system which is always non-negative.

A general time-invariant system can be described by an ordinary differential equation

$$\begin{cases} \dot{x}(t) = f(x(t),\ u(t)) \\ y\ (t) = h(x(t),\ u(t)) \end{cases} \tag{1}$$

where t, $x(t)$, $u(t)$, and $y(t)$ are the time, states, inputs, and output vectors of the system. In some cases, the above model can be estimated by a linear model

$$\begin{cases} \dot{x}(t) = A_C\ x(t) + B_C\ u(t) \\ y\ (t) = C_C\ x(t) + D_C\ u(t) \end{cases} \tag{2}$$

Table 1
The components and performance parameters of the experimental setup shown in Fig. 2.

Component	Company & model number	Description
Load Cell	Omega LCEB-5	Output 3 mV/V nominal, calibration NIST-traceable, 7 mN linearity, 5 mN hysteresis, 3 mN repeatability, compensated temperature range − 15 to 65 °C (0 to 150°F), input resistance 350 Ω + 50/− 3.5 Ω, output resistance 350 Ω ± 3.5 Ω, construction high-carbon steel, 1.5 m (5′) insulated 4-conductor shielded color-coded cable.
ADC	SparkFun HX711	24-bit, settling time 400 ms, 10 sample per second, operation voltage 2.7 V– 5 V (3.3 was used), simultaneous 50 and 60 Hz supply rejection, operation temperature range: − 40 to + 85 °C, Input common mode rejection 100 dB.
DAC	Texas Instrument TLV5628	8-bit voltage output DACs, 3.3 single supply operation, settling time 10 μs.
SPI bus	NI USB-8452	SPI master interface with clock rates up to 50 MHz, compatible with Windows 7/Vista/XP/2000.
Op-Amp	Texas Instrument OPA2241	2 channels, supply voltage 2.7–36 V, rail-to-rail in to V-Out, GBW 0.035 MHz, slew rate 0.01 V/μs, max offset voltage @ 25C 0.25 (mV), offset Drift 0.4 μV/C, CMRR 124 dB, operating temperature range − 40 to 85 C.
BJT	STMicroelectronics TIP 122	DC current gain 1000, max collector current 5 A, max base current 0.12 A, emitter cut-off current 2 mA, collector cut-off current 0.5 mA, temperature − 65 to 150 °C, max collector-emitter voltage 100 v, max collector-base voltage 100v, max emitter-base voltage 5 V.
Power Supply	Topward 6306D	Output voltage 0–30 V, output current 0–33A, load regulation 0.01% + 2 mV, line regulation 0.01% + 2 mV, ripple & noise < 1mVrms, digital display accuracy full-scale 3% < 0.1% + 2d, output impedance < 2mΩ + 2 μH, series regulation 0.3% + 10 mV.
Mechanical Spring	McMaster 9044K85	Type extension, end type loop, material music-wire steel, overall length 1.286″, length inside ends 1.25″, outside diameter 0.24″, outside diameter tolerance −0.003″ to 0.003″, wire diameter 0.018″, extended length 4.686″, extended length inside ends 4.65″, load, lbs. min. 0.11 maximum 1.18, rate 0.30 lbs./in., rate tolerance −0.02 to 0.02 lbs./in.

where A_C, B_C, C_C, and D_C are constant matrices. Subscript C indicates the variable reflects a model in the continuous time domain. These equations require continuous force measurement and applying continuous voltage; however, researchers commonly use a digital controller such as a microcontroller, DSP, computational board, etc. that work in discrete time. In other words, researchers use digital sensors or analog to digital converters to measure states of systems, which read the physical signals with a samplings time. The sampling time depends on hardware characteristic. Thus, in practice, the states of the systems are available only in discrete time (sampling time T). By changing the differential equations to difference equations, the model is stated as

$$\begin{cases} x[n+1] = A_D\, x[n] + B_D\, u[n] \\ y[n] = C_D\, x[n] + D_D\, [n] \end{cases} \quad (3)$$

where $x[n]$, $u[n]$, and $y[n]$ are states, inputs, and output vectors of the system at time $t = nT$ and A_D, B_D, C_D, and D_D are constant matrices, and subscript D indicates the discrete time domain. The input of the TCP muscle is electrical power ($P[n] = \frac{v^2[n]}{R[n]} \geq 0$), where $R[n]$ is resistance of the muscle in time step n, and $v[n]$ is applied voltage in time step n. The resistance is always a real positive number ($R[n] \geq R_0 > 0$). The resistance value depends on length, area and temperature of the TCP. To reduce the cost of the controller hardware, in this paper, we assume that the resistance is constant. Without this assumption, a current sensor and a power ADC are required. Therefore, the input of the system defined as

$$u[n] := v^2[n] \geq 0. \quad (4)$$

This means the input to the TCP muscle system is always positive, and controlled actuation only occurs in the pulling direction. The TCP actuator in this paper are homochiral and cannot push or apply compressive force against load; it can only contract upon heating [18]. In this work, we must rely on heat dissipation and load for negative actuation. This leads to a hybrid-linear controller [44], i.e. $u[n] = \tilde{u}[n]\, H(\tilde{u}[n])$, where $H(.)$ is Heaviside function, $\tilde{u}[n]$ is controller output, and $u[n]$ is the applied voltage square (v^2) in time step n. The $\tilde{u}[n]$ may be negative when the desired force is less than the measured force in case of the classical controllers.

As stated earlier, a prediction error method was used to estimate the parameters of the discrete-time state space model. Fig. 3(a) shows the different order discrete-time, state space models, 1st order to 5th order, along with experimentally measured force response corresponding to a square wave voltage input. Fig. 3(b) shows the evaluation on different magnitude of desired force that are obtained experimentally and from the 1st order model. We measured the force for long time (80 s) to capture steady-states. The oscillation come from disturbance and noises which is common in practice.

Table 2 shows the estimation parameters with 97.7% fitness to estimation data and 8.7e-6 MSE in self-evaluation and 90% fitness in cross-evaluation. The fitness will increase if hysteresis, friction, spring, and mass are added to the model. The 90% fitness of the model is sufficient to use a linear controller, and a nonlinear controller is not needed. This model is simple, which makes controller design easier.

Table 2
Example of muscle (model) parameter in Fig. 3.

Symbol	Value	Symbol	Value
A_C	−0.1837	A_D	0.9639
B_C	0.004313	B_D	0.0008469
C_C	1	C_D	1
D_C	0	D_D	0
Length	110 mm	T	0.2 s
Resistance	11.0 Ω	DC gain	0.02348 N/V^2

Table 3
Muscle fabrication parameter in Fig. 3.

Parameter	Value	Parameter	Value	Parameter	Value
Fabricating force	1.75 N	Annealing force	2.25 N	Training force	2.25 N
Annealing cycles	5	Annealing current	0.4 A	Annealing periods	50 s
Training cycles	5	Training current	0.4 A	Training periods	50 s
Final strain	4%	Annealing duty cycles	50%	Training duty cycles	50%

4. Controllers

4.1. Classical controller

The simplest way to control the force of the muscle is to use an open-loop controller consisting of a gain equal to the inverse of the DC gain of the muscle. The main problem of the open-loop controller is that it does not change the rise time of the system. A muscle rise time depends on the precursor material, its fabrication process, and the geometry whether it is 1-ply, 2-ply or 3-ply. Here, the response time of the 1-ply TCP is 20 s as seen in Fig. 3. The speed can be increased by using a simple closed-loop controller (Fig. 4), i.e. a proportional controller. However, the proportional controller results in a steady-state error. Therefore, Yip and Niemeyer used a combination of the open-loop and closed-loop, feedforward-proportional controller, to achieve a high speed and low steady-state error (Fig. 4) [41, 42]. The main disadvantage of a feedforward-proportional controller is its sensitivity to the model parameters, especially the DC gain of the muscle. As mentioned in the modeling section, the estimated parameters have error up to 10%. Therefore, determining the exact DC gain of the muscle is

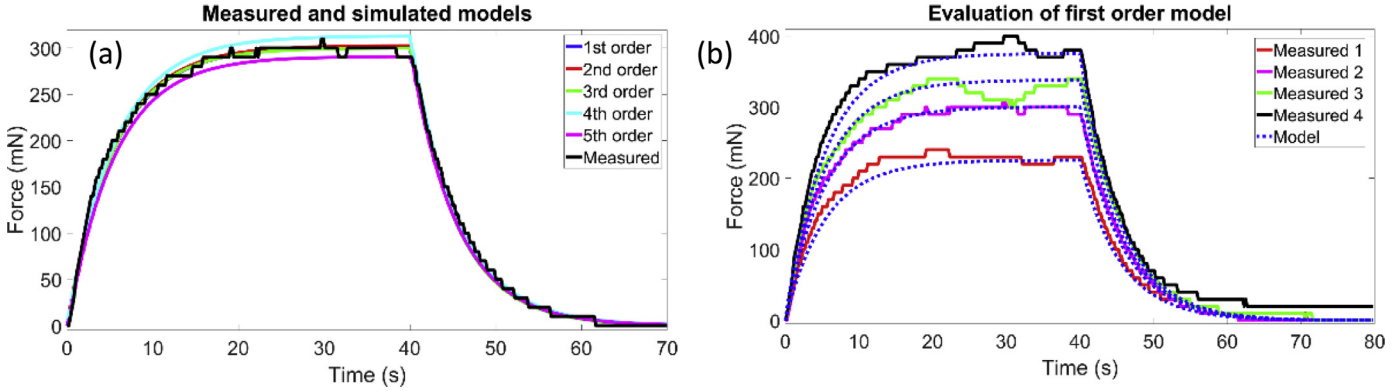

Fig. 3. Modeling of the muscle with discrete time state space models in response to voltage square (V2) input: (a) comparison of different ordered of system (b) evaluation of first order model.

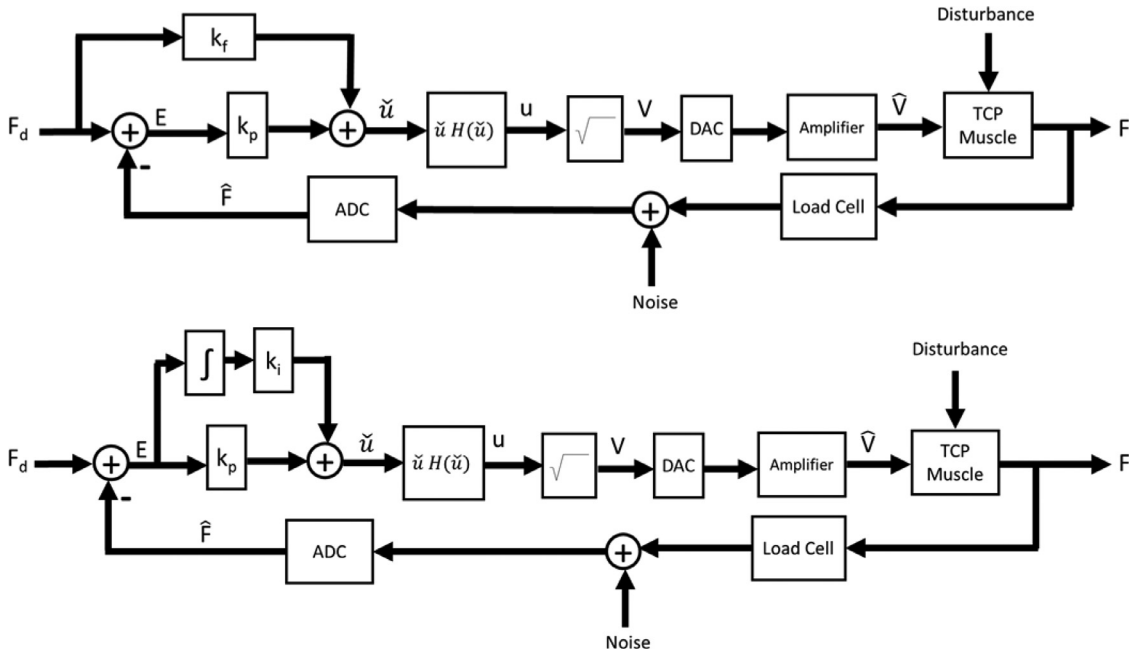

Fig. 4. Function block diagram of closed loop system with feedforward-proportional (FP) controller and proportional-integral (PI) controller.

impossible because the TCP muscle has some nonlinearity, which depends on other un-modeled signals.

In this paper, a proportional-integral (PI) controller is suggested (as illustrated in Fig. 4) to regulate the force of the muscle. Instead of using a feedforward gain to compensate the steady-state error, the Riemann integral of the error is used in the control law. PI controller is robust to the model parameter uncertainties when the system model is passive. More precisely, the muscle force converges to the desired force even if the parameters of the PI controller, i.e. k_p and k_i, slightly change.

4.2. Fuzzy controller

A human can describe his or her feelings and experiences in the control of muscle by using linguistic words. An analogous approach can be used in the control of a TCP muscle. There exist several well-known methods to design an inference system by linguistic rules. Adaptive neuro-fuzzy inference system (ANFIS) method uses neural networks [45–47], whereas Mamdani's methods only use the linguistic words in both condition statements and conclusion statements [48–54]. For example: if the force error is large and integral of error is also large, then the voltage of muscle is very large. Another method uses linguistic words just in conditional statements and uses equations in conclusion statements.

The latter view is known as Takagi–Sugeno–Kang (TSK) [55–65] view of a fuzzy inference system (FIS). Fig. 5a shows the function block diagram of a general Takagi–Sugeno–Kang view of a fuzzy inference system. As we know, the sensor outputs or the inputs of the controller are real numbers, not linguistic words. Therefore, membership functions should be defined to map membership values to each value of sensors. The membership value is a real value between zero and one. Fig. 5b shows an example of membership functions for control of the TCP muscles by using the error signal of the controlled variable, force in this case. The speed of the PI controller can increase if the maximum voltage is given to the muscle when the error is larger than some threshold. A better way is to smoothly transition between the maximum voltage and a proportional–integral controller. Takagi–Sugeno–Kang view of fuzzy inference system is used for the smooth transition (Fig. 6a). Let us define three linguistic rules:

- Rule 1: If error is negative large, then $u[n] = 0$
- Rule 2: If error is small, then $u[n] = k_p^{TSK} e[n] + k_i^{TSK} \sum_{m=0}^{n-1} e[m]T$
- Rule 3: If error is positive large, then $u[n] = Maximum\ voltage\ square$

where T is sampling time, $e[n]$ is the error in time step n, k_p^{TSK} and k_i^{TSK} are constants. When the error is negative, the voltage should be zero (Rule 1) because the muscle is actuated by voltage squared, which is positive semi-definite. Rule 2 is applied when the error is small, which sets the output ($u[n]$) to a proportional–integral controller. A shorter response time will be obtained by giving high voltage when the error is positive large (Rule 3). The end user defines the large set, in this case, the force error according to the properties of the TCP muscle and the intended application. The Gaussian function is used as membership function in the control of many actuators such as permanent magnet direct current (PMDC) motor [66], brushless dc (BLDC) motor [67], voice coil motor [68], stepping motor [69], induction motor [70]. Alternative functions could be used but we preferred the Gaussian function as a membership function for TCP muscle for the reasons mentioned above. It is given by:

$$g(x, m, \sigma) = e^{-\frac{(x-m)^2}{2\sigma^2}}, \tag{5}$$

where x is input, m is mean, and σ is standard deviation. Membership functions are defined as follows:

- The membership function of negative large is defined as

$$\mu_{NL}(e[n]; m_{NL}, \sigma_{NL}) = \begin{cases} 1 & e[n] \le m_{NL} \\ g(e[n], m_{NL}, \sigma_{NL}) & e[n] > m_{NL} \end{cases} \tag{6}$$

- The membership function of small is defined a

$$\mu_S(e[n]; m_S, \sigma_S) = g(e[n], 0, \sigma_S) \tag{7}$$

- The membership function of positive large is defined as

$$\mu_{PL}(e[n]; m_{PL}, \sigma_{PL}) = \begin{cases} g(e[n], m_{PL}, \sigma_{PL}) & e[n] < m_{PL} \\ 1 & e[n] \ge m_{PL} \end{cases} \tag{8}$$

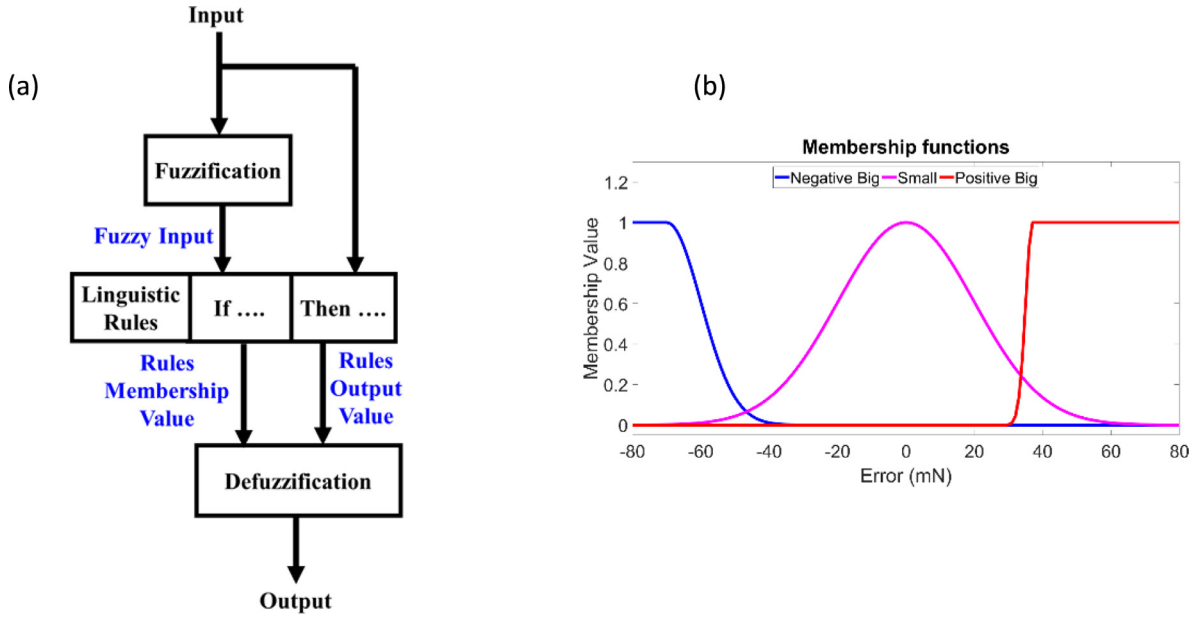

Fig. 5. fuzzy inference system (FIS) (a) Takagi–Sugeno–Kang (TSK) view of a general (b) example of membership function for controlling a TCP muscles using force error signal.

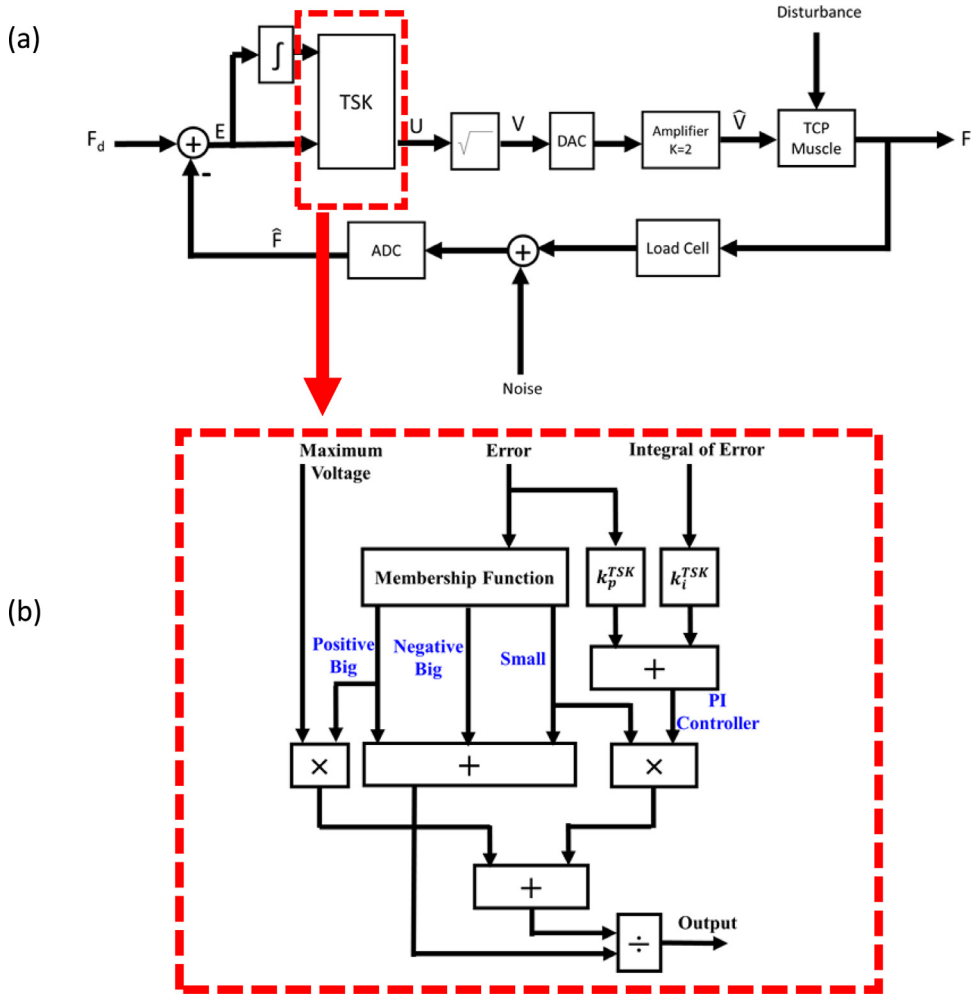

Fig. 6. Takagi–Sugeno–Kang (TSK) controller (a) whole function block diagram and (b) inside of TSK block.

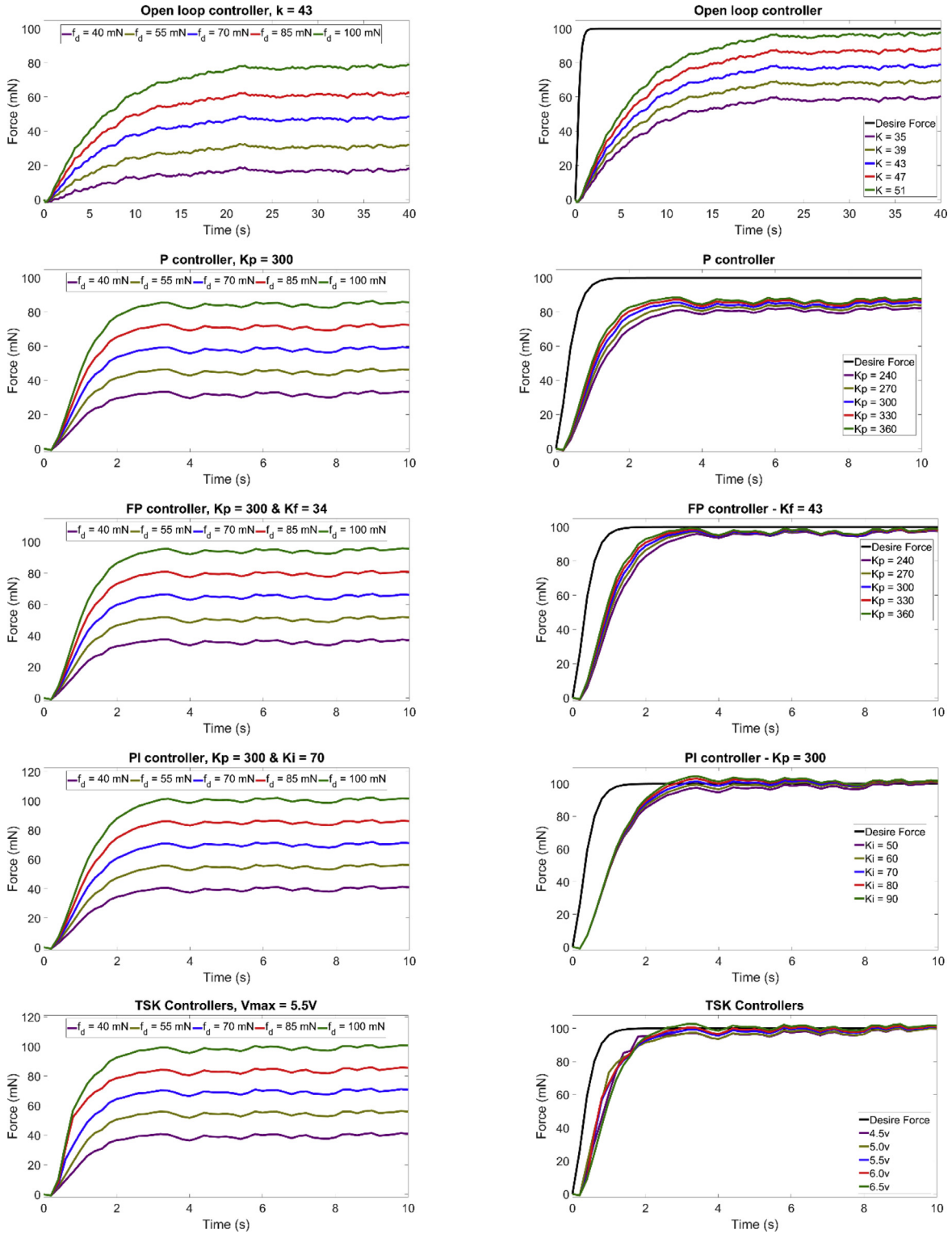

Fig. 7. Simulation result with consideration of 4 mN uniformly distributed noise and 50 mN uniformly distributed disturbance. The left side is for different desired force and the right side is for 100 mN desired force.

where $e[n]$ is the error which is defined in Eq. (6), $m_{NL}$and σ_{NL} are mean and standard deviation of "negative large" set, σ_S is the standard deviation of "small" set, m_{PL} and σ_{PL} are mean and standard deviation of "positive large" set. The μ_{NL}, μ_S, and μ_{PL} are membership functions of negative large, small, and positive large respectively. The value of membership functions μ_{NL}, μ_S, and μ_{PL} for error, $e[n]$, range from zero to one which shows how much a specific error belong to negative large, small, and positive large. On a membership function curve, if the membership value is equal to zero, then it means that the error does not belong to that curve. On the other hand, if the membership value is equal to one, the error completely belongs to that set. One of the membership functions for the TCP muscle is illustrated in Fig. 5b, where the error is in horizontal axis, and the membership value is in the vertical axis. In many cases, there will be overlap. For example, in

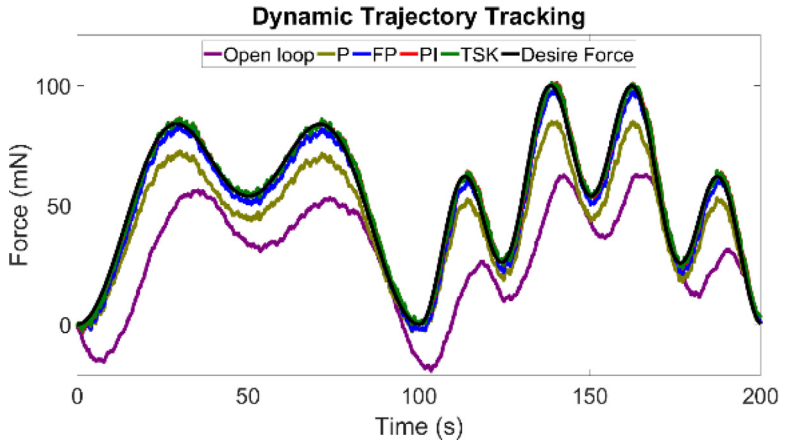

Fig. 8. Simulation of tracking an arbitrary generated trajectory.

Fig. 5b, if the error is −50 mN, the negative large has 0.18 and small has 0.05 membership value. These magnitudes will be used in Eq. (12) to determine the output of the controller. In contrast to the probability, the summation of membership functions can be any positive real number, i.e. the summation is not limited to be equal to positive one [48–53]. The weighted average is used as a defuzzifier to calculate the output of the controller, which is given as:

$$u(e[n], h[n]) = \frac{\mu_S(k_p^{TSK} e[n] + k_i^{TSK} h[n]) + \mu_{PL} V_{max}^2}{\mu_{NL}[n] + \mu_S[n] + \mu_{PL}[n]} \tag{9}$$

where V_{max}^2 is a constant, which is equal to upper limit of the TCP muscle, and the maximum of voltage obtained from the power circuit. This voltage is given by end user, and it depends on the muscle and hardware. The $h[n]$ is Riemann integral of error.

To optimally tune the TSK, one can use the cost function $J = \mathscr{E}_r\{\mathscr{E}_N\{ e[n]^2\}$, where $\mathscr{E}_N$ is the expected value over a trajectory, and $\mathscr{E}_r$ is the expected value over all physically possible trajectories. By substituting Eqs. (3) and (9) in the cost function we obtain

$$J = \mathscr{E}_r\left\{\mathscr{E}_N\left\{r[n+1] - a\, y[n] - b\, \frac{\mu_S(k_p^{TSK} e[n] + k_i^{TSK} h[n]) + \mu_{PL} V_{max}^2}{\mu_{NL}[n] + \mu_S[n] + \mu_{PL}[n]}\right\}\right\}. \tag{10}$$

Note that Eq. (10) cannot be solved analytically, but by using Monte Carlo method [71, 72], we can approximate the cost function as

$$J \approx \hat{J} = \frac{1}{M}\frac{1}{N}\sum_{m=1}^{M}\sum_{n=0}^{N-1}\left(r[n+1] - a\, y[n] - b\, \frac{\mu_S(k_p^{TSK} e[n] + k_i^{TSK} h[n]) + \mu_{PL} V_{max}^2}{\mu_{NL}[n] + \mu_S[n] + \mu_{PL}[n]}\right). \tag{11}$$

The optimal parameters of the TSK controller minimize Eq. (11), which is non-linear and can have multiple local optima. Therefore, gradient-based optimization methods cannot be used. The parameters can be tuned by using evolutionary algorithms such as genetic algorithms [73], the bee colony algorithm [74], particle swarm optimization [75], cuckoo search [76], bat algorithm [77], or imperialist competitive algorithm [78]. Also, the parameters can be tuned by stochastic optimization methods such as random search [79] and cross-entropy method (CEM) [80, 81].

5. Results and discussion

5.1. Numerical simulation

Fig. 7 shows the system response (first-order discrete-time LTI state space with parameters shown in Table 2) in presence of noise (4 mN uniformly distributed) and disturbance (50 mN uniformly distributed). The disturbance could be from two sources. One source of disturbance could be from environments such as air flow. The other source could be due to the simplification of non-linear model to linear model and also from higher order to lower order ODE. In the first set of simulation (the left column of Fig. 7), we kept the controller parameters constant and studied the different desired forces, 40 mN, 55 mN, 70 mN, 85 mN, and 100 mN. The desired input was shaped to have 1 s rise time. The open-loop system could not reach the desired trajectory and had a large rise time. The proportional controller is faster than open-loop controller; however, it cannot compensate for the disturbance error. The expected value of the steady-state error is less than the expected value of the disturbance. However, still there is a significant amount of error. The effect of noise is completely vanished. The ratio of steady-state error to the desired force is constant (in contrast to the open-loop controller). The feedforward-proportional controller (FP) shows less steady-state error than the proportional controller (P). However, the expected value of the steady-state error is not zero. The proportional–integral controller (PI) and TSK controller converged to the desired trajectory. The TSK controller reaches to the steady-state response faster than the other controllers.

In the next set of simulations (right side in Fig. 7), we kept the desired trajectory constant and simulated the systems with different controller parameters. The open-loop controllers had large errors, because the open-loop controllers do not consider the disturbance, which is uniformly distributed with magnitude of 50 mN for this simulation. The settling time of the open-loop system is higher than other controllers because the open-loop controllers do not affect the system characteristic root, i.e. the system pole. The proportional controller had error that varied widely with k_p. The error and rise time decreased as the gain increased. In practice, k_p is bounded because the voltage of power supply is limited. Therefore, there is a lower bound for the steady-state error of the proportional controller. The feedforward-proportional controller has lower steady-state error than proportional controller. The feedforward gain, k_f, cannot compensate the disturbance. The expected value of the steady-state error of feedforward-proportional controller does not converge to zero. The rise time of actuator decreases as k_p increased. The effect of k_p on the expected value of the steady-state is negligible. The proportional–integral controllers compensated the steady-state error that includes the error caused by disturbance. Some overshoots appeared as the k_i increased. The TSK

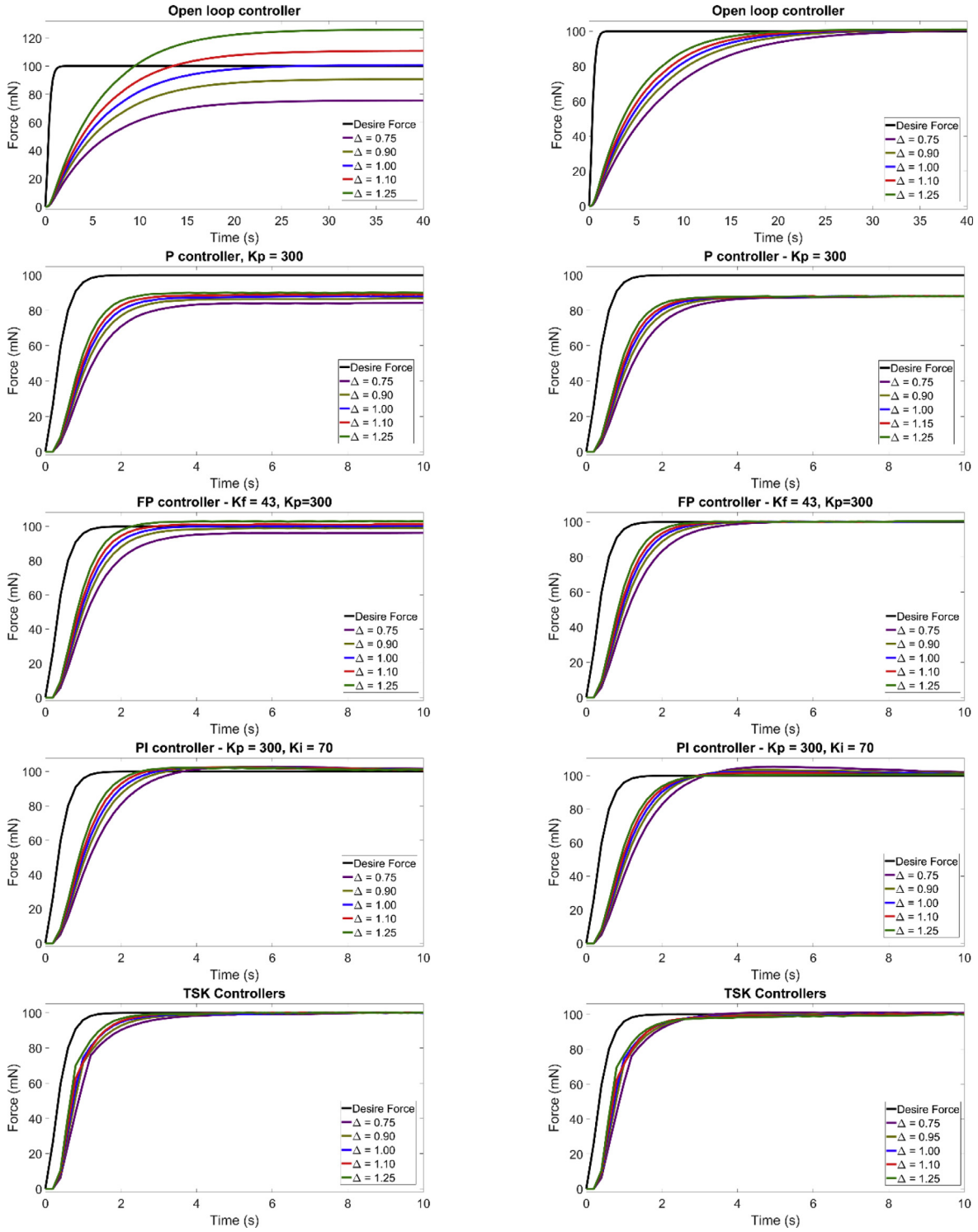

Fig. 9. Simulation result of sensitivity of the controllers to DC gain of the muscle (left column) and pole of the muscle (right column).

shows the fastest response, besides the steady-state error converged to zero. The rise time of system with TSK controller decreased as the upper bound of voltage increased.

Fig. 8 demonstrates the system response with an arbitrary trajectory of force, which is positive throughout the time 200 s. The gain of the open-loop controller is 43, which is the inverse of DC gain of the simulated actuator. The open-loop controller (goes to negative force, less force than the initial, because of disturbance (50 mN uniformly distributed). The proportional controller ($K_p = 300$) has a significant amount of error. The disturbance is almost compensated with the proportional controller. What remains can be decreased by selecting a higher value for K_p. The feedforward-proportional controller ($K_f = 43$ and $K_p = 300$) shows a little error. The proportional–integral ($K_p = 300$ and $K_i = 70$) and TSK controllers (V_{max}=5.5v) can track the trajectory with minimum error. There is no significant difference between the behavior of the PI and TSK controller in this simulation because the desired trajectory is smooth such that the error is always small. According to the linguistic rules, the TSK behaves like a PI controller when the error is small.

Fig. 9 shows other two set of simulations. In the third set of

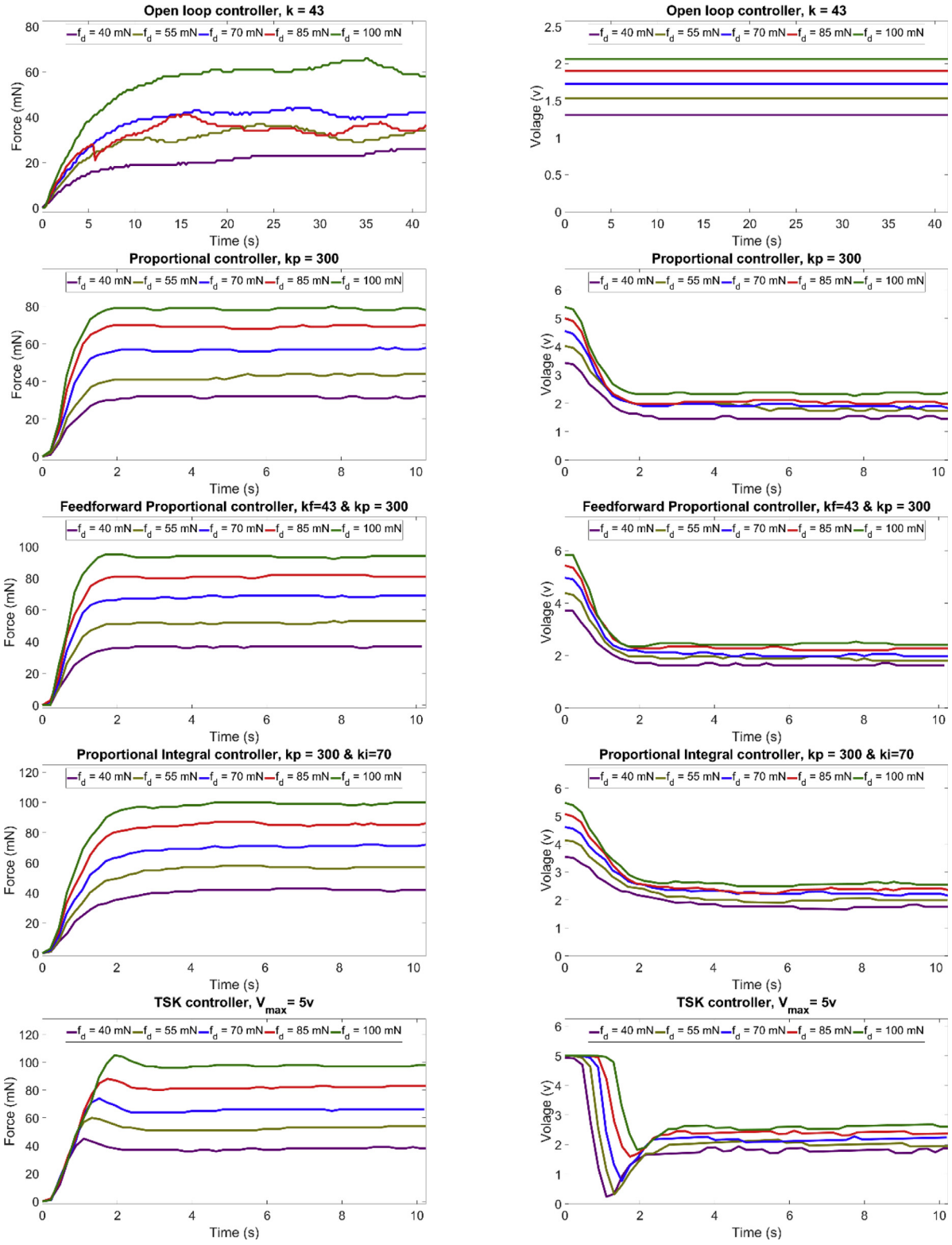

Fig. 10. Experiment result for a 110 mm 1-ply TCP muscle.

simulations (left column of Fig. 9), the sensitivity of the controllers to the gain of the model is illustrated. The Δ indicates the multiplication constant for DC gain of the model, i.e. $K_{DC} = \Delta\ K_0$, where K_0 is nominal DC gain. In this analysis, the noise and disturbance are assumed to be zero. The open-loop controller shows maximum sensitivity to the steady-state in response to the change in DC gain (equal to one). For example, when the DC gain increased by 25%, the steady-state force is also increased by 25%. The proportional controller ($K_p = 300$) and feedforward-proportional controller ($K_f = 43$ and $K_p = 300$) show sensitivity to change in DC gain. The rise time and steady-state error of this controller are decreased by increasing the DC gain of the simulated actuator. The feedforward-proportional controller ($K_f = 43$ and $K_p = 300$) is also sensitive to change in DC gain of the simulated actuator. Similar to the proportional controller, the rise time of the

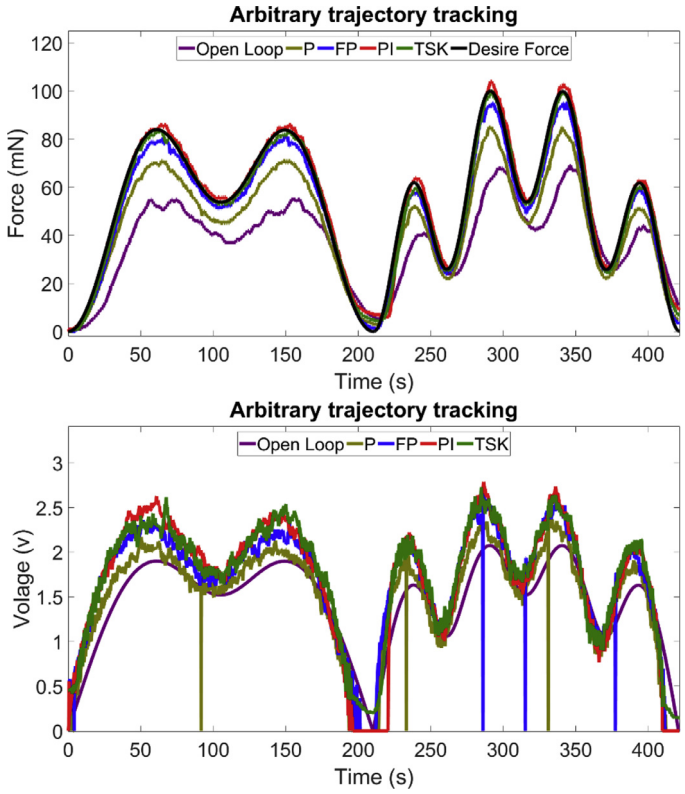

Fig. 11. Experiment result for a 110 mm TCP muscle arbitrary desired trajectory.

Table 4
Control performances in Fig. 10.

Controller	K_{rise}	E_{rise} (mN)	Overshoot (mN)	Effort (v^2)	K_{ss}	E_{ss} (mN)
Open-loop	73	69	5	311	201	49
P	8	55	1	132	8	18
FP	8	49	1	151	8	5
PI	11	44	1	179	11	1
TSK	9	54	8	184	12	2

feedforward-proportional controller decreases as the DC gain increases. The steady-state force of the feedforward-proportional controller increases as the DC gain increases such that it becomes greater than the desired force (i.e. negative error). The rise time of proportional–integral controller ($K_p = 300$ and $K_i = 70$) is affected by Δ. However, the steady-state error converged to zero in all cases, i.e. it is not sensitive. The TSK controller shows minimum sensitivity in comparison with other controllers. The rise time of TSK controller is also increased by increasing the DC gain.

In the fourth set of simulations (left column of Fig. 9), sensitivity of the controllers with respect to the pole of the actuator model is studied. The controller parameters were selected exactly the same as the second study. The noise and disturbance were zero similar to the third study. The $\Delta > 1$ means the pole gets closer to the unit circle in discrete-time frequency domain, i.e. slower open-loop response. The rise time magnitudes of all controllers are decreased as multiplication factor Δ increased. The steady-state errors of the all controllers were not sensitive to the pole of the actuator. The proportional controller is affected more than other controllers. However, overshoot appears in proportional–integral and TSK controller when the Δ was more than 1.

5.2. Experimental results

Experimental results for 1-ply TCP muscle of length 110 mm and diameter of 0.8 mm is shown in Fig. 10. The trajectory is a step input with 40 mN, 55 mN, 70 mN, 85 mN, and 100 mN. The disturbance mostly come from lab air condition and noises mostly come from lab natural vibration. We did not enclose the muscle to compare controllers in presence of noise and disturbance, which exist in practice. The first order system with a single integrator for PI control together constitute a second order system.

MATLAB's Robust Control Toolbox was used with the second order model to find the H_∞ optimal gains $K_p = 99$ and $K_i = 26$. For comparison purposes, we also used the MATLAB Control System Designer to find another set of constants K_p and K_i by setting the tuning method to robust response time with maximum speed and robustness. This returned gains of $K_p = 464$ and $K_i = 16$. The high proportional gain broke the muscle. Therefore, we set the $K_p = 300$ (see Fig. 10 experimental

Table 5
Control performances in Fig. 11, for regulating arbitrary force trajectory.

Controller	Maximum Absolute Error, Force, (mN)	Median Absolute Error, Force, (mN)	Mean Absolute Error, Force, (mN)	STD absolute Error, Force, (mN)	Maximum output, Voltage, (V)	Median output, Voltage, (V)	Mean output, Voltage, (V)	STD output, Voltage, (V)
Open-loop	38.07	15.40	15.89	9.88	4.30	2.46	2.30	1.16
P	19.01	9.34	8.87	4.48	5.70	2.80	2.61	1.42
FP	9.90	2.97	3.31	2.10	7.14	3.42	3.20	1.69
PI	15.65	1.82	2.26	2.05	7.77	3.55	3.40	1.98
TSK	8.74	1.72	2.05	1.69	7.43	3.65	3.42	1.87

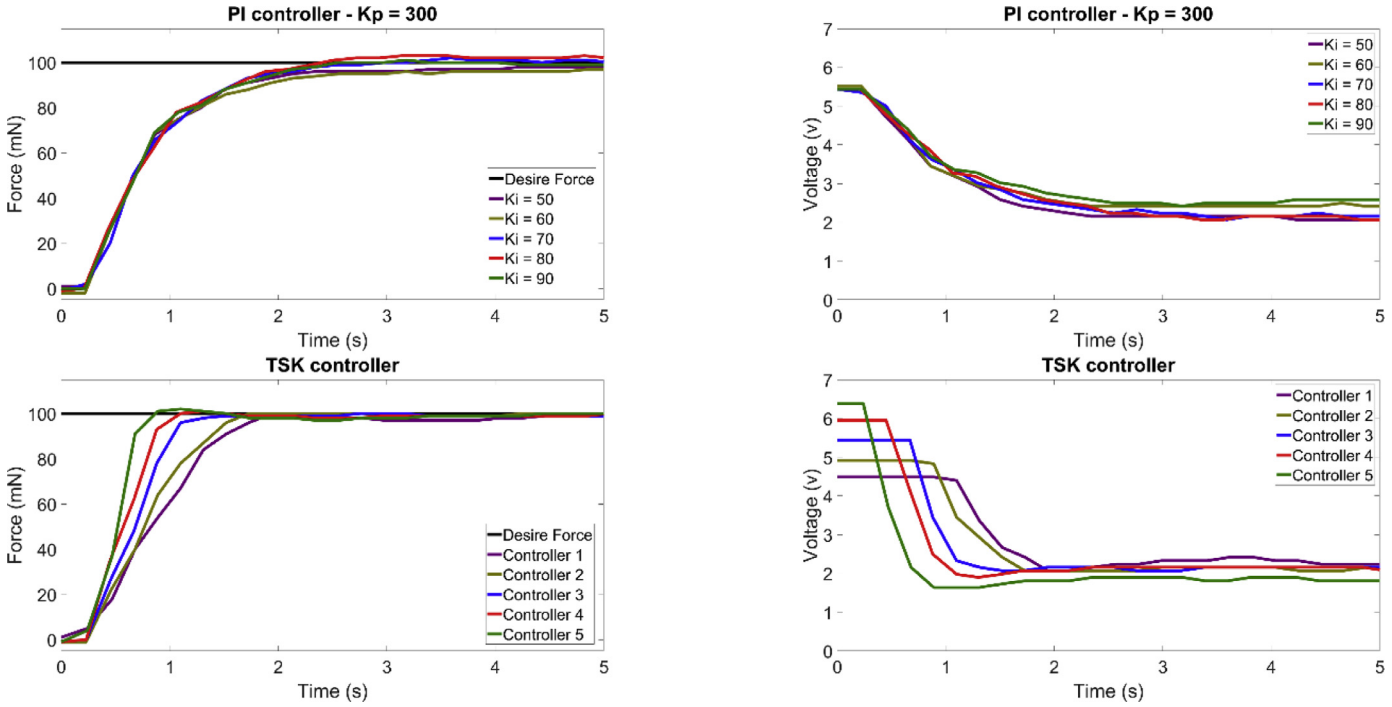

Fig. 12. Experiment result for a 110 mm TCP muscle.

Table 6
TSK controller parameter in the experiment for Fig. 12.

Symbol	Cont. 1	Cont. 2	Cont. 3	Cont. 4	Cont. 5
V_{max}	4.5	5.0	5.5	6.0	6.5
m_{NB}	−0.1	−0.1	−0.1	−0.1	−0.1
σ_{NB}	0.010	0.010	0.010	0.010	0.010
σ_S	0.017	0.017	0.020	0.025	0.040
m_{PB}	0.020	0.030	0.037	0.045	0.100
σ_{PB}	0.002	0.002	0.002	0.002	0.010
k_p	350	360	375	370	190
k_i	60	65	75	88	80

data), between the values set by both control design approaches. We then incremented $K_i = 26$ in a series of trials to get faster response (1 s ideally) without overshooting. The final value is $K_i = 70$. The achievable response time was 2.2 s (Fig. 10). The same K_p used in PI controller was used for the FP and P controllers. The force response are illustrated in the left column, and the corresponding voltages for different controllers are in the right side of Fig. 10. The open-loop controller gives fixed voltage regardless of the force error. Therefore, the output is more affected by disturbance. These experimental results confirm the simulation results obtained earlier in the simulation. The importance of the TSK controller is evident in Fig.10; for desired force magnitude, the TSK controller maintains the maximum voltage 5 V whereas the other controllers, except open-loop, increase the voltage magnitude higher than 5 V. This can be clearly seen on the right side of Fig. 10.

The experimental result in tracking an arbitrary trajectory is shown in Fig 11. The open-loop controller could not compensate the disturbances and noises. The feedforward-proportional controller shows less error as compared to the proportional controller. The proportional–integral controller has more delay than other controllers. Therefore, in some portions, the proportional–integral works better than the feedforward-proportional controller; while, in the other portions the feedforward-proportional controller track better. The TSK controller works better than other controllers. The open-loop controller applies a smooth changing voltage because it does not care about noise and disturbance. Several times, the applied voltage to the muscle by the proportional and feedforward-proportional controllers suddenly drop to zero and return back because the computed errors were negative at that moment. A summary is provided in Table 4, showing the control performance for different controllers while tracking arbitrary trajectory. Further, the statistics of the results in Fig. 11 are quantified and presented in Table 5. This indicates that the TSK controller has the lowest maximum absolute, mean error and standard deviation, which confirms the advantage of this controller.

Another set of experimental result is presented in Fig. 12 for comparing the effect of parameters of proportional–integral and TSK controller along with the voltages provided to the muscle to control the force. The result shows that both the proportional–integral controller and Takagi–Sugeno–Kang controller successfully regulated the force of the muscle. The proportional–integral controller has two gains, k_p and k_i. Initial speed increases as k_p increases. However, the k_p does not significantly affect the settling time. Although the settling time can decrease by increasing k_i, it will cause overshoot if the k_i pass a threshold. The overshoot is not acceptable in some robotic and mechatronic systems. In addition, choosing high gain for k_p and k_i can cause instability, which must be avoided. Takagi–Sugeno–Kang (TSK) controllers have many parameters as compared to proportional–integral controllers.

Therefore, TSK controller takes significantly more time to find the proper parameters values. Also, it is notable that the TSK controller parameters depend on maximum voltage. As the maximum voltage increases, the positive large membership function would shift to the right, and the small membership function becomes flatter (larger σ). Table 6 shows the TSK controller parameters obtained by trial and error during the experiments. The experimental results show that in TCP muscle, TSK controllers have faster response than proportional–integral controllers because the voltage is maximum when the error is large at the beginning. By increasing the peak voltage, the speed of TSK controllers will increase. However, exceeding a certain level of “maximum voltage” parameter causes an overshoot in the force response, and the magnitude of this overshoot grows by further increase in the voltage (controller 5 in Fig. 12). Decreasing force takes more time than increasing the force because we can only heat the muscle by electrical power, the cooling part is not controlled in the current study, and it is

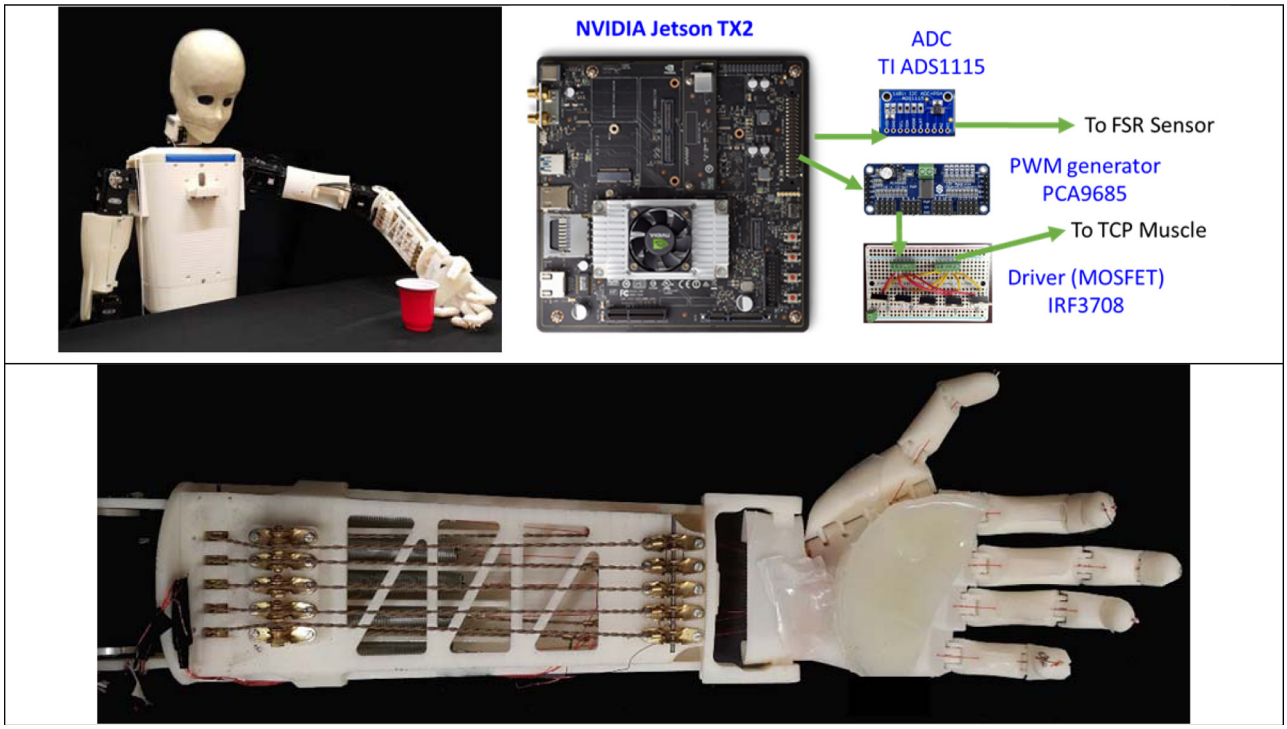

Fig. 13. Application of TCP muscle in a humanoid robot (HBS) include hand circuits controlled by NVIDIA Jetson TX2 developer kit.

governed by convective heat transfer. Therefore, overshoot significantly increases the settling time. Thus, overshoot must be avoided by parameter tuning.

In short, the controller parameters affect the closed-loop system behavior. The k_p parameter of the PI controller affects the transient behavior of the system. The transient time decreases as k_p increases and the applied voltage in the sharp part of a trajectory (like step or square wave) increases as k_p increases. However, higher applied voltage breaks the TCP muscle (discussed in section 5.2). Therefore, there is a physical upper-bound limit for the parameter k_p. The pair of k_p and k_i affect the behavior of the closed-loop system after rise time and before settling time. Increasing k_i up to a certain value (generally unknown, but dependent on k_p) reduces the settling time, and increasing k_i after this value adds overshoot and increases the settling time (as seen in Fig. 7, the 4th row in the right side). The V_{max} of the TSK controller depends on the physical characteristic of TCP actuator such as electrical resistance, length, etc., as well as the hardware including power supply and DAC. The other parameters of the TSK controller are highly nonlinear, which is shown in Eq. (10). For tuning the PI parameters, we suggest using H_∞ method to find the most robust values. For tuning the TSK parameters, we suggest solving Eq. (11) in simulation and then fine-tuning with trial and error. If the user wants to tune the TSK parameters in shorter time (sub-optimal), he/she can find the k_p and k_i with H_∞ and substitute in Eq. (11) and find other parameters with cross-entropy method (CEM) [80, 81] in simulation, then do fine tuning with covariance matrix adaptation evolution strategy (CMA-ES) [82-84] with real system.

6. Application

Currently, many humanoid robots use rotary electrical motors, such as permanent magnet DC motors, brushless motors, stepper motors, etc. Although rotary electrical motors are energy efficient, they are too bulky for some applications. Therefore, substituting the rotary electrical motor with artificial muscle is beneficial. The TCP muscles can be used in the humanoid robot as linear actuators. We have developed a humanoid robot HBS-1 [20] that uses several Dynamixel servomotors as well as shape memory alloy (SMA) actuators that were later replaced by TCP muscles [20]. The latest version of the robot, HBS 2.0, that is shown in Fig. 13, consists of 5 TCP muscles for actuation of fingers. One side of each TCP muscle is connected to a linear spring and the other side is connected to a tendon. This design provides one degree of freedom for each finger.

The HBS 2.0 uses an NVIDIA Jetson TX2 developer kit as the main computational board, which run Robotics Operation System (ROS) on top of Linux Ubuntu 16.04 LTS. The kit has Serial Peripheral Interface (SPI), Inter-Integrated Circuit (I^2C), Universal Asynchronous Receiver-Transmitter (UART), and Controller Area Network (CAN) bus, which enables it to communicate to most of the digital to analog converters, analog to digital converters, and Pulse Width Modulation (PWM) drivers available on market. Therefore, the HBS2.0 can measure force by using force sensitive resistor (FSR) and can drive the TCP muscles by either PWM or DAC.

Each object has its own mechanical property such as stiffness and coefficient of friction. Therefore, the amount of force that the hand should apply to the object directly depends on the objects. Thus, controlling the force of each finger is required. The proportional-integral controller, which is explained in this paper, can be used for this purpose as it shows the robustness to variation of the muscle model parameter. Also, the Takagi–Sugeno–Kang controller can be used for a faster response.

7. Conclusion

In this paper, we presented the modeling of TCP muscles using discrete-time state space systems, and the model parameters were estimated using prediction error method. Experiments were performed, and a first order model. showed a better fitting accuracy as compared to higher order models. These experiments are consistent with some of the control works on TCP muscles. The proposed model showed a fitness better than 90%, which is sufficient for controller design.

In the literature, feedforward-proportional controllers have been used to regulate the force of the muscle. Sensitivity to model parameters is the main disadvantage of the feedforward-proportional controller. In this work, instead of a feedforward-proportional controller, a

proportional–integral controller was used. The proportional–integral controller is faster than the previously discussed controllers, and its steady-state error converges to zero. The proportional–integral controller is robust to the model parameters, especially the DC gain of the model, which is crucial because the models always contain some uncertainties.

Moreover, the Takagi–Sugeno–Kang (TSK) view of a general fuzzy inference system (FIS) is used to design a force controller that is even faster than the proportional–integral controller. In this controller, the muscle receives the maximum actuation voltage when the error is positive large. On the other hand, the muscle receives the proportional–integral controller output when the error is small, and the voltage will be zero when the error is negative large. The transitions between these three rules are smooth. The Gaussian membership function was used as a fuzzifier, and a weighted average method is used as defuzzifier. The experiment shows the advantages of the fuzzy controller over the proportional–integral controller.

The proposed controller can be used in many mechatronic and robotic systems which use TCP muscles as actuating mechanism. For example, a humanoid robot must provide some amount force to objects during picking and placing. The amount of force depends on object's mechanical property such as stiffness and coefficient of friction. The proposed controller can be used in the humanoid robots that are actuated by the TCP muscles.

In this paper, tuning the TSK parameters (by trial and error) presented a notable challenge. Online tuning of TSK parameter (fuzzy adaptive controller) should be addressed in the future. Transferring the tuned parameters of a TSK controller for a TCP muscle to a new controller for another TCP muscle (similar, but not identical) and further fine-tuning the parameters will be studied in the future. Controlling a pair of actuators (to create bidirectional behavior), controlling the actuator along with active cooling (fan, or cooling water), studying the behavior of muscle in response to pulse (less than 10 ms), and pulse control of the actuator will all be considered in the future.

References

[1] Full RJ, Meijer K. Metrics of natural muscle function. Chapter 2001;3:73–89.
[2] Hill AV. The heat of shortening and the dynamic constants of muscle. Proc R Soc London B 1938:136–95. Place: Published.
[3] Hunter IW, Lafontaine S. A comparison of muscle with artificial actuators. Solid-state sensor and actuator workshop, 1992. 1992. p. 178–85. 5th Technical Digest., IEEE, IEEE, Place: Published.
[4] Josephson R. Contraction dynamics and power output of skeletal muscle. Ann Rev Physiol 1993;55:527–46.
[5] Baughman RH. Playing nature's game with artificial muscles. Science 2005;308:63–5.
[6] Ahn KK, Kha NB. Modeling and control of shape memory alloy actuators using Preisach model, genetic algorithm and fuzzy logic. Mechatronics 2008;18:141–52.
[7] Romano R, Tannuri EA. Modeling, control and experimental validation of a novel actuator based on shape memory alloys. Mechatronics 2009;19:1169–77.
[8] Sayyaadi H, Zakerzadeh MR. Position control of shape memory alloy actuator based on the generalized Prandtl–Ishlinskii inverse model. Mechatronics 2012;22:945–57.
[9] Zakerzadeh MR, Sayyaadi H. Precise position control of shape memory alloy actuator using inverse hysteresis model and model reference adaptive control system. Mechatronics 2013;23:1150–62.
[10] Lee J, Jin M, Ahn KK. Precise tracking control of shape memory alloy actuator systems using hyperbolic tangential sliding mode control with time delay estimation. Mechatronics 2013;23:310–7.
[11] Ko J, Jun MB, Gilardi G, Haslam E, Park EJ. Fuzzy PWM-PID control of cocontracting antagonistic shape memory alloy muscle pairs in an artificial finger. Mechatronics 2011;21:1190–202.
[12] Hu J, Zhu Y, Huang H, Lu J. Recent advances in shape–memory polymers: Structure, mechanism, functionality, modeling and applications. Prog Polym Sci 2012;37:1720–63.
[13] Romasanta L, Lopez-Manchado M, Verdejo R. Increasing the performance of dielectric elastomer actuators: a review from the materials perspective. Prog Polym Sci 2015;51:188–211.
[14] Zhang J-F, Yang C-J, Chen Y, Zhang Y, Dong Y-M. Modeling and control of a curved pneumatic muscle actuator for wearable elbow exoskeleton. Mechatronics 2008;18:448–57.
[15] Lin C-J, Lin C-R, Yu S-K, Chen C-T. Hysteresis modeling and tracking control for a dual pneumatic artificial muscle system using Prandtl–Ishlinskii model. Mechatronics 2015;28:35–45.
[16] Ba DX, Ahn KK. Indirect sliding mode control based on gray-box identification method for pneumatic artificial muscle. Mechatronics 2015;32:1–11.
[17] Song C, Xie S, Zhou Z, Hu Y. Modeling of pneumatic artificial muscle using a hybrid artificial neural network approach. Mechatronics 2015;31:124–31.
[18] Haines CS, Lima MD, Li N, Spinks GM, Foroughi J, Madden JD, Kim SH, Fang S, de Andrade MJ, Göktepe F. Artificial muscles from fishing line and sewing thread. Science 2014;343:868–72.
[19] Wu L, de Andrade MJ, Saharan LK, Rome RS, Baughman RH, Tadesse Y. Compact and low-cost humanoid hand powered by nylon artificial muscles. Bioinspiration Biomimetics 2017;12:026004.
[20] Wu L, Larkin M, Potnuru A, Tadesse Y. Hbs-1: a modular child-size 3d printed humanoid. Robotics 2016;5:1.
[21] Saharan L, de Andrade MJ, Saleem W, Baughman RH, Tadesse Y. iGrab: hand orthosis powered by twisted and coiled polymer muscles. Smart Mater Struct 2017;26:105048.
[22] Tadesse Y, Wu L, Saharan LK. Musculoskeletal system for bio-inspired robotic systems. Mech Eng 2016;138:S11.
[23] Kim SH, Lima MD, Kozlov ME, Haines CS, Spinks GM, Aziz S, Choi C, Sim HJ, Wang X, Lu H. Harvesting temperature fluctuations as electrical energy using torsional and tensile polymer muscles. Energy Environ Sci 2015;8:3336–44.
[24] Huo W, Mohammed S, Moreno JC, Amirat Y. Lower limb wearable robots for assistance and rehabilitation: a state of the art. IEEE Syst J 2016;10:1068–81.
[25] Madden JD, Kianzad S. Twisted lines: artificial muscle and advanced instruments can be formed from nylon threads and fabric. IEEE Pulse 2015;6:32–5.
[26] Sharafi S, Li G. A multiscale approach for modeling actuation response of polymeric artificial muscles. Soft Matter 2015;11:3833–43.
[27] Zhang J, Iyer K, Simeonov A, Yip MC. Modeling and inverse compensation of hysteresis in supercoiled polymer artificial muscles. IEEE Rob Autom Lett 2017;2:773–80.
[28] Zhang J, Simeonov A, Yip MC. Three-dimensional hysteresis compensation enhances accuracy of robotic artificial muscles. Smart Mater Struct 2018.
[29] Xiang C, Yang H, Sun Z, Xue B, Hao L, Rahoman MA, Davis S. The design, hysteresis modeling and control of a novel SMA-fishing-line actuator. Smart Mater Struct 2017;26:037004.
[30] Weijde Jvander, Smit B, Fritschi M, van de Kamp C, Vallery H. Self-sensing of deflection, force, and temperature for joule-heated twisted and coiled polymer muscles via electrical impedance. IEEE/ASME Trans Mechatron 2017;22:1268–75.
[31] Arakawa T, Takagi K, Tahara K, Asaka K. Position control of fishing line artificial muscles (coiled polymer actuators) from nylon thread. Electroactive polymer actuators and devices (EAPAD). International Society for Optics and Photonics; 2016. 97982W, Place: Published; 2016.
[32] Takagi K, Arakawa T, Takeda J, Masuya K, Tahara K, Asaka K. Position control of twisted and coiled polymer actuator using a controlled fan for cooling. Electroactive polymer actuators and devices (EAPAD). International Society for Optics and Photonics; 2017:101632V. Place: Published; 2017.
[33] Edmonds BP, Trejos AL. Stiffness control of a nylon twisted coiled actuator for use in mechatronic rehabilitation devices. Rehabilitation robotics (ICORR), 2017 international conference on, IEEE. 2017. p. 1419–24. Place: Published.
[34] Abbas A, Zhao J. A physics based model for twisted and coiled actuator. Robotics and automation (ICRA), 2017 IEEE international conference on. IEEE; 2017. p. 6121–6. Place: Published.
[35] Zhao J, Abbas A. A low-cost soft coiled sensor for soft robots. ASME 2016 dynamic systems and control conference. American Society of Mechanical Engineers; 2016. Place: PublishedV002T026A006-V002T026A006.
[36] Tang X, Liu Y, Li K, Chen W, Zhao J. Finite element and analytical models for twisted and coiled actuator. Mater Res Express 2018;5:015701.
[37] Karami F, Tadesse Y. Modeling of twisted and coiled polymer (TCP) muscle based on phenomenological approach. Smart Mater Struct 2017;26:125010.
[38] Masuya K, Ono S, Takagi K, Tahara K. Feedforward control of twisted and coiled polymer actuator based on a macroscopic nonlinear model focusing on energy. IEEE Rob Autom Lett 2018.
[39] Suzuki M, Kamamichi N. Displacement control of an antagonistic-type twisted and coiled polymer actuator. Smart Mater Struct 2018.
[40] Suzuki M, Kamamichi N. Control of twisted and coiled polymer actuator with anti-windup compensator. Smart Mater Struct 2018.
[41] Yip MC, Niemeyer G. High-performance robotic muscles from conductive nylon sewing thread. Robotics and automation (ICRA), 2015 IEEE international conference on. IEEE; 2015. p. 2313–8. Place: Published.
[42] Yip MC, Niemeyer G. On the control and properties of supercoiled polymer artificial muscles. IEEE Trans Rob 2017;33:689–99.
[43] Jafarzadeh M, Wu L, Tadesse Y. System identification of force of a silver coated twisted and coiled polymer muscle. ASME 2017 International mechanical engineering congress and exposition. American Society of Mechanical Engineers; 2017. Place: PublishedV04BT05A027-V004BT005A027.
[44] Liberzon D. Switching in systems and control. Springer Science & Business Media; 2012. PlacePublished.
[45] Petković D, Issa M, Pavlović ND, Zentner L, Ćojbašić Ž. Adaptive neuro fuzzy controller for adaptive compliant robotic gripper. Expert Syst Appl 2012;39:13295–304.
[46] Petković D, Pavlović ND, Ćojbašić Ž, Pavlović NT. Adaptive neuro fuzzy estimation of underactuated robotic gripper contact forces. Expert Syst Appl 2013;40:281–6.
[47] Petković D, Shamshirband S, Anuar NB, Sabri AQM, Rahman ZBA, Pavlović ND. Input displacement neuro-fuzzy control and object recognition by compliant multi-fingered passively adaptive robotic gripper. J Intell Rob Syst 2016;82:177–87.
[48] Fakoor M, Kosari A, Jafarzadeh M. Humanoid robot path planning with fuzzy Markov decision processes. J Appl Res Technol 2016;14:300–10.

[49] Fakoor M, Kosari A, Jafarzadeh M. Revision on fuzzy artificial potential field for humanoid robot path planning in unknown environment. Int J Adv Mechatron Syst 2015;6:174–83.
[50] Jin Y. Advanced fuzzy systems design and applications. Physica, Published; 2012. Place.
[51] Ross TJ. Fuzzy logic with engineering applications. John Wiley & Sons, Published; 2009. Place.
[52] Nguyen HT, Walker EA. A first course in fuzzy logic. CRC press, Published; 2005. Place.
[53] Klir G, Yuan B. Fuzzy sets and fuzzy logic. Prentice hall New Jersey, Published; 1995. Place.
[54] Duțu L-C, Mauris G, Bolon P. A fast and accurate rule-base generation method for Mamdani fuzzy systems. IEEE Trans Fuzzy Syst 2018;26:715–33.
[55] Sugeno M, Kang G. Structure identification of fuzzy model. Fuzzy Sets Syst 1988;28:15–33.
[56] Sugeno M. Industrial applications of fuzzy control. Elsevier Science Inc., Published; 1985. Place.
[57] Sugeno M. An introductory survey of fuzzy control. Inf Sci 1985;36:59–83.
[58] Takagi T, Sugeno M. Derivation of fuzzy control rules from human operator's control actions. IFAC proceedings volumes. 16. 1983. p. 55–60.
[59] Sugeno M, Takagi T. Multi-dimensional fuzzy reasoning. Fuzzy Sets Syst 1983;9:313–25.
[60] Takagi T, Sugeno M. Fuzzy identification of systems and its applications to modeling and control. IEEE Trans Syst Man Cybern 1985;15:396–404.
[61] Ding B, Pan H. Dynamic output feedback-predictive control of a Takagi–Sugeno model with bounded disturbance. IEEE Trans Fuzzy Syst 2017;25:653–67.
[62] Li H, Wang J, Du H, Karimi HR. Adaptive sliding mode control for Takagi–Sugeno fuzzy systems and its applications. IEEE Trans Fuzzy Syst 2018;26:531–42.
[63] Wei Y, Qiu J, Lam H-K. A novel approach to reliable output feedback control of fuzzy-affine systems with time delays and sensor faults. IEEE Trans Fuzzy Syst 2017;25:1808–23.
[64] Wiktorowicz K. Design of state feedback adaptive fuzzy controllers for second-order systems using a frequency stability criterion. IEEE Trans Fuzzy Syst 2017;25:499–510.
[65] Zuo H, Zhang G, Pedrycz W, Behbood V, Lu J. Granular fuzzy regression domain adaptation in Takagi–Sugeno fuzzy models. IEEE Trans Fuzzy Syst 2017.
[66] Zaki AM, El-Bardini M, Soliman F, Sharaf MM. Embedded two level direct adaptive fuzzy controller for DC motor speed control. Ain Shams Eng J 2015.
[67] Rubaai A, Young P. Hardware/software implementation of fuzzy-neural-network self-learning control methods for brushless DC motor drives. IEEE Trans Ind Appl 2016;52:414–24.
[68] Lin C-M, Li H-Y. Adaptive dynamic sliding-mode fuzzy CMAC for voice coil motor using asymmetric Gaussian membership function. IEEE Trans Ind Electron 2014;61:5662–71.
[69] Chen C-S. TSK-type self-organizing recurrent-neural-fuzzy control of linear microstepping motor drives. IEEE Trans Power Electron 2010;25:2253–65.
[70] Wang S-Y, Tseng C-L, Chiu C-J. Design of a novel adaptive TSK-fuzzy speed controller for use in direct torque control induction motor drives. Appl Soft Comput 2015;31:396–404.
[71] Peña A, Bonet I, Lochmuller C, Chiclana F, Góngora M. An integrated inverse adaptive neural fuzzy system with Monte-Carlo sampling method for operational risk management. Expert Syst Appl 2018.
[72] Rubinstein RY, Kroese DP. Simulation and the Monte Carlo method. John Wiley & Sons, Published; 2016. Place.
[73] Chin CS, Lin WP. Robust genetic algorithm and fuzzy inference mechanism embedded in a sliding-mode controller for an uncertain underwater robot. IEEE/ASME Trans Mechatron 2018;23:655–66.
[74] Habbi H, Boudouaoui Y, Karaboga D, Ozturk C. Self-generated fuzzy systems design using artificial bee colony optimization. Inf Sci 2015;295:145–59.
[75] Haji VH, Monje CA. Fractional order fuzzy-PID control of a combined cycle power plant using Particle Swarm Optimization algorithm with an improved dynamic parameters selection. Appl Soft Comput 2017;58:256–64.
[76] Ding X, Xu Z, Cheung NJ, Liu X. Parameter estimation of Takagi–Sugeno fuzzy system using heterogeneous cuckoo search algorithm. Neurocomputing 2015;151:1332–42.
[77] Premkumar K, Manikandan B. Bat algorithm optimized fuzzy PD based speed controller for brushless direct current motor. Eng Sci Technol Int J 2016;19:818–40.
[78] Al Khaled A, Hosseini S. Fuzzy adaptive imperialist competitive algorithm for global optimization. Neural Comput Appl 2015;26:813–25.
[79] Méndez V, Campos D, Bartumeus F. Random search strategies. Stochastic foundations in movement ecology. Springer; 2014. p. 177–205.
[80] Anisimov D, Dang TS, Banerjee S. Design and implementation of fuzzy-PD controller based on relation models: a cross-entropy optimization approach. Eur Phys J Spec Top 2017;226:2393–406.
[81] Haber RE, Beruvides G, Quiza R, Hernandez A. A simple multi-objective optimization based on the cross-entropy method. IEEE Access 2017;5:22272–81.
[82] Beyer H-G, Sendhoff B. Simplify your covariance matrix adaptation evolution strategy. IEEE Trans Evol Comput 2017;21:746–59.
[83] Iruthayarajan MW, Baskar S. Covariance matrix adaptation evolution strategy based design of centralized PID controller. Expert Syst Appl 2010;37:5775–81.
[84] Kadhar KMA, Baskar S. Covariance matrix adaptation evolution strategy based design of fixed structure robust H∞ loop shaping controller. Appl Soft Comput 2015;34:337–48.